

Calculation of optical gain in AlGaN quantum wells for ultraviolet emission

Cite as: AIP Advances **10**, 095307 (2020); <https://doi.org/10.1063/5.0021890>

Submitted: 16 July 2020 . Accepted: 18 August 2020 . Published Online: 03 September 2020

Bernd Witzigmann , Friedhard Römer, Martin Martens, Christian Kuhn, Tim Wernicke , and Michael Kneissl



View Online



Export Citation



CrossMark

ARTICLES YOU MAY BE INTERESTED IN

[Milliwatt power 233 nm AlGaN-based deep UV-LEDs on sapphire substrates](#)


Applied Physics Letters **117**, 111102 (2020); <https://doi.org/10.1063/5.0015263>

[Origin of carrier localization in AlGaN-based quantum well structures and implications for efficiency droop](#)

Applied Physics Letters **117**, 102107 (2020); <https://doi.org/10.1063/5.0018885>


[Impact of defects on Auger recombination in c-plane InGaN/GaN single quantum well in the efficiency droop regime](#)

Applied Physics Letters **116**, 222106 (2020); <https://doi.org/10.1063/5.0004321>



NEW!

Sign up for topic alerts
New articles delivered to your inbox



Calculation of optical gain in AlGaIn quantum wells for ultraviolet emission

Cite as: AIP Advances 10, 095307 (2020); doi: 10.1063/5.0021890

Submitted: 16 July 2020 • Accepted: 18 August 2020 •

Published Online: 3 September 2020



View Online



Export Citation



CrossMark

Bernd Witzigmann,^{1,a)}  Friedhard Römer,¹ Martin Martens,² Christian Kuhn,² Tim Wernicke,²  and Michael Kneissl²

AFFILIATIONS

¹Department of Electrical Engineering and CINSaT, University of Kassel, Wilhelmshöher Allee 71, 34121 Kassel, Germany

²Technische Universität Berlin, Institute of Solid State Physics, Hardenbergstr. 36, EW6-1, 10623 Berlin, Germany

^{a)} Author to whom correspondence should be addressed: witzigma@uni-kassel.de

ABSTRACT

Stimulated emission from AlGaIn based quantum wells (QWs) emitting at ultraviolet wavelengths is investigated theoretically. Maxwell–Bloch equations in the second Born approximation are solved self-consistently with the Poisson equation. The valence band dispersion is obtained from a 6-band $k\cdot p$ -model. For a QW emitting at around 270 nm with a thickness of 2.2 nm, an estimated FWHM of 10 meV for homogeneous broadening and an excitonic red shift of 100 meV are extracted under typical laser conditions. From a comparison to experimental data of stimulated emission, an inhomogeneous broadening energy of 39 meV FWHM is evaluated. Calculations show that high TE gain can be achieved for thin QWs around 2 nm thickness in a multiple QW arrangement or for single QWs thicker than 6 nm.

© 2020 Author(s). All article content, except where otherwise noted, is licensed under a Creative Commons Attribution (CC BY) license (<http://creativecommons.org/licenses/by/4.0/>). <https://doi.org/10.1063/5.0021890>

I. INTRODUCTION

Aluminum gallium nitride (AlGaIn) heterostructures have enabled semiconductor light emitting diodes in the ultraviolet (UV) spectrum, down to the UVC range.¹ AlGaIn based UV lasers with high power densities have a great potential in various applications such as water purification, general sterilization, and sensing systems. Realizing electrically injected lasers in the UV spectrum has remained a challenge, and devices with pulsed operation at 272 nm emission and 25 kA/cm² threshold current density have been reported.² Several obstacles need to be overcome for improving the performance. High optical losses are introduced by magnesium induced absorption in the cladding and the absorptive p-contacts.³ The acceptor activation energy of AlGaIn layers rises with Al content; therefore, claddings with high optical index contrast are poor p-conductors at the same time.² Thick ternary AlGaIn layers lead to alloy fluctuations that change the carrier dynamics and emission from the quantum wells.⁴ Finally, polarization charges at the well–barrier interfaces lead to reduced matrix elements for radiative transitions, and in multiple quantum well (QW) systems, they create barriers for carrier injection.

In this paper, the configuration for high optical gain from AlGaIn QWs is investigated. The focus is on QW thickness, and the calculations exhibit that for thin quantum wells in the order of 2 nm, electron confinement can be critical, while for thicker QWs, the polarization field reduces the matrix element. Design proposals for high gain with both thin and thick QWs are shown, and gain is calculated. Finally, the impact of inhomogeneous broadening is demonstrated quantitatively by detailed comparison to the experiment. The theoretical method solves the optical Bloch equations in the second Born–Markov approximation⁵ in order to calculate spectral gain in AlGaIn QWs emitting in the ultraviolet spectral range.

II. SIMULATION MODEL

The band structure of the active region is calculated using a 6-band $k\cdot p$ method for the hole states, including band mixing of the heavy-hole, light-hole, and split-off bands.⁶ A single-band model calculates the electron band dispersion. The $k\cdot p$ method is iterated with the nonlinear Poisson equation, including the stationary charges at interfaces and compositional gradients arising from the

polar hexagonal crystal. Strain relaxation is calculated based on a biaxial continuum model.⁶ Optical gain is obtained from a semi-classical theory,^{5,7} consisting of the microscopic polarization and the optical matrix element. The microscopic polarization results from the semiconductor Bloch equations, including many-body effects from the Coulomb interaction in the Hamiltonian. The polarization dephasing rates are calculated within the second Born approximation in the Markovian limit.⁵ Both the $\mathbf{k} \cdot \mathbf{p}$ -Poisson-solver and the solution of the Bloch equations have been implemented within our research.⁸ The main signatures of many-body interactions are homogeneous broadening, excitonic effects, and bandgap renormalization in the gain spectra. The simulation model employs a set of material parameters for the calculation. The $\mathbf{k} \cdot \mathbf{p}$ method requires band structure data for AlGaIn taken from Rinke *et al.*⁹ and polarization data taken from Dreyer *et al.*¹⁰ The valence band splitting energy parameters have been taken from Carvalho *et al.*¹¹ and are close to experimentally determined values.

III. SINGLE QUANTUM WELL vs SUPERLATTICE

At first, a single AlGaIn QW vs a superlattice with AlGaIn barriers is studied. The Al mole fraction of the barrier is 90%, and the well mole fraction is chosen for emission around 270 nm. In addition to the choice of bandgap energy in the barrier, the polarization fields have an impact on the stimulated emission as well. At hetero-interfaces, the charge density σ_{int} creating these fields results from the difference in polarization \vec{P} ,¹⁰

$$\sigma_{int} = (\vec{P}_{tot}^1 - \vec{P}_{tot}^0) \cdot \vec{n}, \quad (1)$$

where the total polarization consists of the piezoelectric part and the spontaneous part. For the case of a QW between two barriers, there is a net charge at the QW-barrier interfaces, originating from the piezo and spontaneous polarization. At the other side of the barriers, there are interfaces again, and for those, two scenarios can be identified: a single well between thick barriers creates polarization fields only at the well-barrier interface, in the limit of an infinite barrier (the infinite barrier setup). This leads to a potential drop between the left and right barriers. An illustration is shown in Fig. 1. The

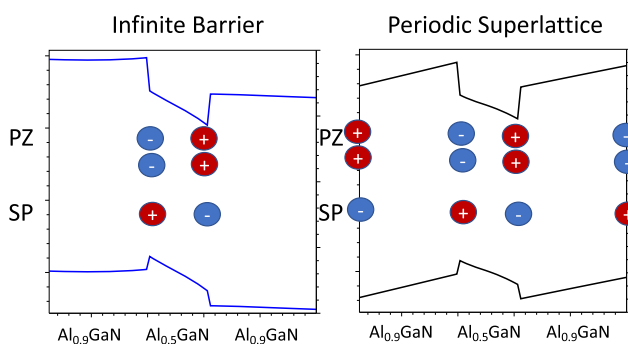


FIG. 1. Conduction and valence band setup for the infinite barrier and periodic superlattice quantum well of thickness 2.2 nm. The interface charges resulting from the piezoelectric (PZ) and spontaneous (SP) polarization fields are shown schematically.

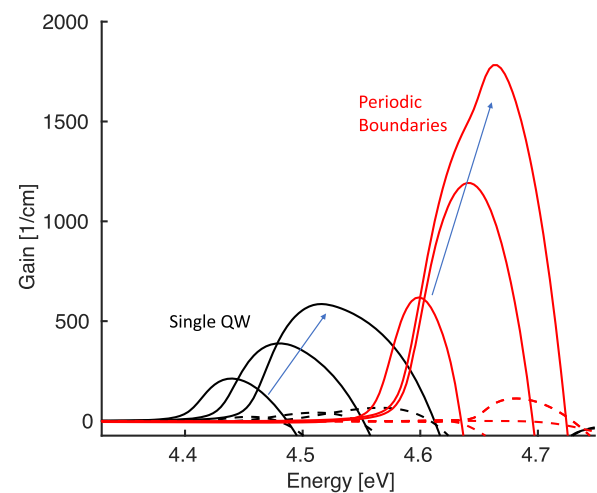


FIG. 2. Material gain of a QW with 2.2 nm thickness emitting at around 270 nm. Black lines: infinite barrier case ($n = p = 5.0, 6.0, 7.0 \times 10^{19} \text{ cm}^{-3}$); red lines: periodic superlattice case ($n = p = 4.0, 5.0, 6.0 \times 10^{19} \text{ cm}^{-3}$); and dashed lines: TM gains.

second case assumes a QW in a periodic superlattice arrangement, where the electric field is present both in the well and in the barrier (Fig. 1, right) due to periodic charge placement. This results in an additional slope of the bands in the barrier.

Figure 2 shows the material gain for the two cases. The mole fraction difference at the well-barrier interface creates charge densities of $\sigma = 1.3 \times 10^{13} \text{ cm}^{-2}$ at the well-barrier interface, resulting in a Stark shift. At well densities of around $5.0 \times 10^{19} \text{ cm}^{-3}$, these charges are only partially screened; nevertheless, a strong gain peak shift is observed in this figure with a rising carrier density. Much smaller material gain is obtained from the infinite barrier model, mainly because of the weak electron confinement at the right well-barrier interface (see Fig. 1, left). In addition, the optical transition energy is $\sim 150 \text{ meV}$ lower, as the effective confinement potential is lower. The larger width in the gain spectrum, compared to the periodic boundary case, is due to narrow sub-band spacing, which favors population of the heavy hole 2 (HH2) sub-band and contributes to gain. For periodic boundaries, the onset of this transition can be seen at the highest density in the plot.

The results indicate that for the AlGaIn system, the inner wells in a multi-QW stack possess an improved electron confinement due to the electric field created from the polarization charge at the neighboring barrier. Material gain is improved by a factor of 4 (see Fig. 2), with an additional red shift of peak gain. With a confinement factor of 4.2%,³ modal gain for a laser is therefore 12 cm^{-1} for the infinite barrier case and 50.0 cm^{-1} for a well in the superlattice case (for a carrier density of $5.0 \times 10^{19} \text{ cm}^{-3}$).

IV. COMPARISON TO EXPERIMENT

In the following, the simulation data are compared to experimental data in order to understand the influence of alloy fluctuations. AlGaIn-based heterostructures were grown by metal-organic

vapor phase epitaxy on defect-reduced AlN/sapphire templates.¹² The laser structures, designed for optical pumping, contain a 500 nm thick $\text{Al}_{0.8}\text{Ga}_{0.2}\text{N}$ bottom cladding layer, a 30 nm thick $\text{Al}_{0.7}\text{Ga}_{0.3}\text{N}$ waveguide, and an unintentionally doped threefold MQW consisting of 2.2 nm thick AlGaN quantum wells and 5 nm thick $\text{Al}_{0.7}\text{Ga}_{0.3}\text{N}$ barriers as well as an 85 nm thick $\text{Al}_{0.7}\text{Ga}_{0.3}\text{N}$ top waveguide. Asymmetric (10.5) x-ray diffraction analyses exhibit a pseudomorphically strained heterostructure without indication for relaxation.¹³ After scribing and cleaving of individual laser bars, the optical gain was determined by the variable stripe length method (VSLM) using a 193 nm emitting ArF excimer laser source with stripe shaped non-resonant excitation. The emitted light from the facet was detected using a fiber-coupled spectrometer. The simulations have been carried out in a single QW setup with the infinite barrier $\text{Al}_{0.7}\text{Ga}_{0.3}\text{N}$ boundaries. Figure 3 shows the experiment (dots) in comparison to the calculations for three different pumping levels. A striking feature of the experimental spectra is the gain maximum staying constant at all three pumping levels. As the excitation of the structure is done optically at the energy above the barrier energy, it is assumed that in the barrier regions, a high carrier density is present, which is able to screen the polarization fields to a large degree. Therefore, the polarization charges in the simulation have been scaled to 20% of the original values to account for the barrier screening effect. This way, the gain peak evolution with carrier density follows the experimentally observed characteristic.

In addition, the experimental data show a much more pronounced spectral broadening compared to the calculation. This can be attributed to the compositional fluctuations in the ternary material.⁸ In order to account for this in the simulation, the gain spectra are convolved with a Gaussian function with a FWHM broadening of σ_{inh} . In the case of the sample under investigation, a broadening of $\sigma_{inh} = 39$ meV is used as a fit parameter.

Spectral broadening of the optical emission is composed of homogeneous and inhomogeneous components. Homogeneous broadening is caused by dephasing of the interband transition due

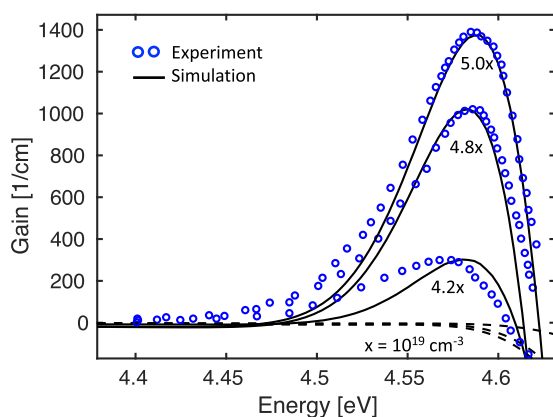


FIG. 3. Comparison of experimental gain (dots) with simulation of TE gain (solid lines and dashed lines are TM polarization). Densities are (from low to high) $n = p = 4.2, 4.8, 5.0 \times 10^{19} \text{ cm}^{-3}$. Simulations include inhomogeneous broadening with a FWHM of 39 meV.

to carrier–carrier and carrier–phonon scattering. In our simulations, carrier–carrier scattering is included within the second Born approximation, phonon effects are neglected. The latter have shown to modify the gain characteristics slightly,¹⁴ which could explain the deviation of experiment and simulation at the low-energy tail. In order to understand the spectral gain shape, the homogeneous broadening energy is extracted from the simulation. This is done by replacing the gain calculation by a free carrier model, as described in Ref. 15. Figure 4 plots the resulting spectral gain for the different models, with the same material parameters and band structure model. At a carrier density of $n = p = 5.1 \times 10^{19} \text{ cm}^{-3}$, the free carrier model gain is peaking at 4.72 eV, while the second Born calculation peaks at 4.61 eV. For the latter, a slightly lower density of $n = p = 5.0 \times 10^{19} \text{ cm}^{-3}$ has been chosen. The free carrier model includes homogeneous broadening with a heuristic hyperbolic secant function, with a FWHM energy of $E_{hom} = 10$ meV. The dashed line in this figure is the free carrier result, shifted to the red by $\Delta E = 110$ meV, with a good match to the second Born result. Three major conclusions can be made: the energy red shift from the bandgap renormalization effect at carrier densities typical for lasing operation is in our case larger than 100 meV. In addition, the peak gain enhancement due to the Coulomb interaction of the carriers is 10% and hence the slight increase in carrier density for the free carrier model. Finally, the homogeneous broadening calculated in the second Born model can be approximated in the free carrier model by a heuristic hyperbolic secant function, with a FWHM energy of $E_{hom} = 10$ meV. With these modifications, the free carrier theory can therefore represent the much more complex many-body calculation reasonably. The dotted line in Fig. 4 shows the experiment, together with the inhomogeneously broadened second Born result.

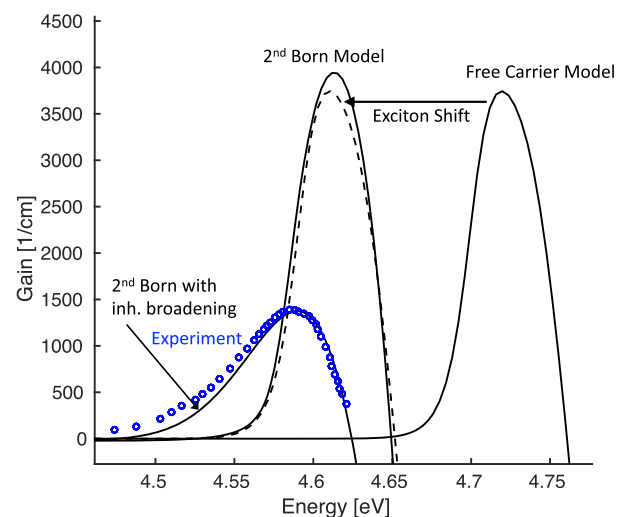


FIG. 4. Comparison of gain models. Right solid curve: free carrier theory (FCT) with a sech-lineshape homogeneous broadening (10 meV FWHM). The second Born calculation has a red shift of $\Delta E = 110$ meV and higher peak gain due to exciton enhancement. Dashed curve: FCT model artificially shifted by ΔE . Dots: experimental data, together with the inhomogeneously broadened second Born result.

V. QUANTUM WELL THICKNESS

Next, the quantum well thickness is varied, and gain is evaluated without inhomogeneous broadening. The thickness of the well varies between 1.5 nm and 9 nm, and the maximum wavelength of the gain spectrum is targeted to 270 nm, with varying Al content. The barriers are $\text{Al}_{0.9}\text{Ga}_{0.1}\text{N}$, and the infinite barrier setup is assumed with respect to the boundary conditions.

Figure 5 shows the maximum of the spectral material gain vs carrier density for the different well thicknesses. For the thin wells at 1.5 nm and 2.0 nm, peak gain rises approximately linearly with density. Besides the increase of the quasi-Fermi level separation, the gradual screening of the polarization charges is responsible for increasing gain. The gain relations for thicknesses of 3.0 nm and 4.0 nm are missing. For these thicknesses, the inversion carrier density is larger than $6.0 \times 10^{19} \text{ cm}^{-3}$ in the simulation. From a thickness of 5.0 nm upward, the inversion density decreases and high differential gain can be observed, which is surprising. The underlying mechanism is illustrated in Fig. 6. The stimulated emission basically comes from inversion from the higher energy levels, in this case, the second conduction band (CB2) and second heavy hole (HH2) band. The lowest eigenstates are still well populated, but they show a low overlap integral between electron and hole states. Their maximum density is located at the well-barrier interface; therefore, they screen the polarization charges and allow a flat band situation in the well center. Therefore, a large overlap integral, i.e., matrix element, can be observed for the CB2 and HH2 eigenstates. High optical gain can therefore only result from the lowest energy states screening the polarization charges and at the higher eigenstates being populated strongly for inversion. An example for this mechanism is shown in Fig. 6 for a well width of 9 nm. The lowest wavefunction for electrons is at the right interface for holes at the left interface. The CB2 and HH2 wavefunction are located in the center of the well.

The matrix elements in momentum space at inversion are shown in Fig. 7. Here, the HH2-CB2 transition dominates; the HH1-CB1 matrix element is negligible and not shown in the graph. For QW thicknesses from 5 nm to 9 nm, the carrier density for large stimulated emission decreases, as shown in Fig. 5. This can be

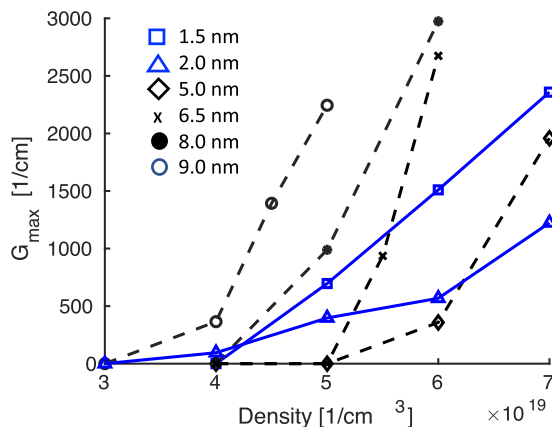


FIG. 5. Maximum material gain for the AlGaIn QW emitting at 270 nm, with $\text{Al}_{0.9}\text{Ga}_{0.1}\text{N}$ barriers. For well thicknesses of 3 nm and 4 nm, no inversion could be calculated at the densities shown.

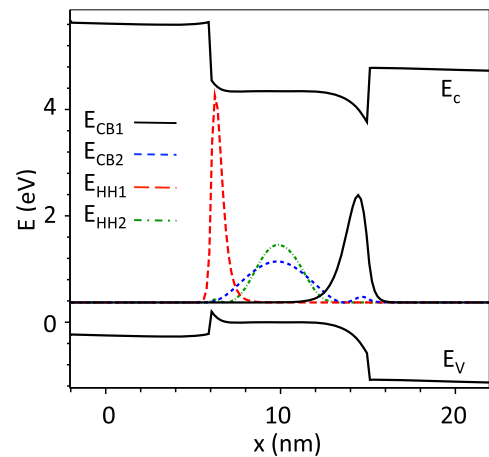


FIG. 6. Conduction and valence band of QW with 9.0 nm thickness emitting at around 270 nm with the AlGaIn barrier containing 90% of Al at a carrier density of $n = p = 5.0 \times 10^{19} \text{ cm}^{-3}$. The red and black lines are the square of the first and second conduction sub-band wave functions, and the blue dashed lines indicate the respective heavy hole wave functions. The lower energy sub-bands peak at the well-barrier hetero-interface, while the second sub-bands peak in the well center with a large overlap.

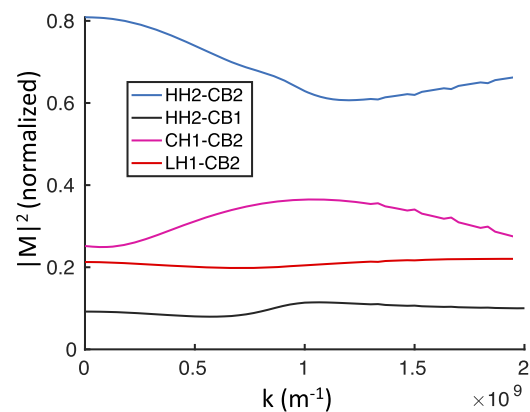


FIG. 7. TE transition matrix element of 9.0 nm QW emitting at 270 nm at a carrier density of $n = p = 5.0 \times 10^{19} \text{ cm}^{-3}$. Optical gain is supported by the CB2-HH2 transition.

explained by the energy spacing of the higher sub-bands, which is decreasing with wider wells. Hence, they are easier to populate even at moderate densities.

VI. CONCLUSION

In summary, optical gain from AlGaIn quantum wells (QWs) emitting at UV wavelengths has been analyzed. The results show that high gain active regions for UV lasers can be realized using two strategies: thin single wells suffer from a reduced electron confinement induced by interface polarization charges, even at carrier

densities that create inversion. In a multiple well or superlattice setup, the periodic electric field from the polarization in the barriers improves the electron confinement considerably with much larger material gain. The second strategy is the use of single wells with larger thicknesses supporting at least two bound electron levels. In this case, population of the lowest energy levels screens the polarization charges, with the higher energy levels providing substantial gain. For a 2.2 nm QW emitting at 270 nm, homogeneous broadening with a sech function of FWHM at 10 meV has been calculated, and a red shift of 110 meV due to bandgap renormalization occurs. Comparison to the experiment shows a Gaussian type inhomogeneous broadening with a FWHM of 39 meV.

DATA AVAILABILITY

The data that support the findings of this study are available from the corresponding author upon reasonable request.

REFERENCES

- ¹M. Kneissl, T.-Y. Seong, J. Han, and H. Amano, "The emergence and prospects of deep-ultraviolet light-emitting diode technologies," *Nat. Photonics* **13**, 233–244 (2019).
- ²Z. Zhang, M. Kushimoto, T. Sakai, N. Sugiyama, L. J. Schowalter, C. Sasaoka, and H. Amano, "A 271.8 nm deep-ultraviolet laser diode for room temperature operation," *Appl. Phys. Express* **12**, 124003 (2019).
- ³M. Martens, C. Kuhn, T. Simoneit, S. Hagedorn, A. Knauer, T. Wernicke, M. Weyers, and M. Kneissl, "The effects of magnesium doping on the modal loss in AlGaIn-based deep UV lasers," *Appl. Phys. Lett.* **110**, 081103 (2017).
- ⁴D. A. Browne, M. N. Fireman, B. Mazumder, L. Y. Kuritzky, Y.-R. Wu, and J. S. Speck, "Vertical transport through AlGaIn barriers in heterostructures grown by ammonia molecular beam epitaxy and metalorganic chemical vapor deposition," *Semicond. Sci. Technol.* **32**, 025010 (2017).
- ⁵W. Chow and S. Koch, *Semiconductor-Laser Fundamentals* (Springer, Berlin, 1999).
- ⁶S. Chuang and C. Chang, "k-p method for strained wurtzite semiconductors," *Phys. Rev. B* **54**, 2491–2506 (1996).
- ⁷O. Hess and T. Kuhn, "Maxwell-Bloch equations for spatially inhomogeneous semiconductor lasers. I. Theoretical formulation," *Phys. Rev. A* **54**, 3347–3359 (1996).
- ⁸B. Witzigmann, V. Laino, M. Luisier, U. T. Schwarz, G. Feicht, W. Wegscheider, K. Engl, M. Fritsch, A. Leber, A. Lell, and V. Härle, "Microscopic analysis of optical gain in InGaIn/GaN quantum wells," *Appl. Phys. Lett.* **88**, 021104 (2006).
- ⁹P. Rinke, M. Winkelnkemper, A. Qteish, D. Bimberg, J. Neugebauer, and M. Scheffler, "Consistent set of band parameters for the group-III nitrides AlN, GaN, and InN," *Phys. Rev. B* **77**, 075202 (2008).
- ¹⁰C. Dreyer, A. Janotti, C. Van de Walle, and D. Vanderbilt, "Correct implementation of polarization constants in wurtzite materials and impact on III-nitrides," *Phys. Rev. X* **6**, 021038 (2016).
- ¹¹L. Carvalho, A. Schleife, F. Fuchs, and F. Bechstedt, "Valence-band splittings in cubic and hexagonal AlN, GaN, and InN," *Appl. Phys. Lett.* **97**, 232101 (2010).
- ¹²M. Martens, "Optical gain and modal loss in AlGaIn based deep UV lasers," Ph.D. thesis, TU Berlin, 2018.
- ¹³C. Kuhn, M. Martens, F. Mehnke, J. Enslin, P. Schneider, C. Reich, F. Krueger, J. Rass, J. B. Park, V. Kueller, A. Knauer, T. Wernicke, M. Weyers, and M. Kneissl, "Influence of waveguide strain and surface morphology on AlGaIn-based deep UV laser characteristics," *J. Phys. D: Appl. Phys.* **51**, 415101 (2018).
- ¹⁴T. Lermer, A. Gomez-Iglesias, M. Sabathil, J. Müller, S. Lutgen, U. Strauss, B. Pasenow, J. Hader, J. V. Moloney, S. W. Koch, W. Scheibenzuber, and U. T. Schwarz, "Gain of blue and cyan InGaIn laser diodes," *Appl. Phys. Lett.* **98**, 021115 (2011).
- ¹⁵S.-L. Chuang, *Physics of Photonic Devices* (Wiley, 2009).